THE GEOLOGICAL SOCIETY OF AMERICA®

Rapid assembly and crystallization of a fossil large-volume silicic magma chamber

Michael P. Eddy[1], Samuel A. Bowring[1], Robert B. Miller[2], and Jeffrey H. Tepper[3]
[1]Department of Earth, Atmospheric and Planetary Sciences, Massachusetts Institute of Technology, Cambridge, Massachusetts 02139, USA
[2]Geology Department, San Jose State University, San Jose, California 95192, USA
[3]Geology Department, University of Puget Sound, Tacoma, Washington 98416, USA

ABSTRACT

The rates at which large volumes of eruptible, silicic (>65 wt% SiO_2) magma (magma chambers) are assembled, as well as their longevity in the upper crust, remain controversial. This controversy is due, in part, to a missing record of granitoid plutonic complexes that represent large fossil upper crustal magma chambers. We present new geologic mapping and high-precision U-Pb zircon geochronology from the Eocene Golden Horn batholith in Washington State, USA. These data reveal that the batholith was constructed as a series of sills over 739 ± 34 k.y. Topographic relief of >2 km permits volume estimates for 4 of the sills, the largest of which, a >424 km^3 rapakivi granite, was emplaced over 26 ± 25 k.y. at a rate of ~0.0125 km^3/yr. This rate exceeds those needed to build large, silicic magma chambers in thermal models, and we suggest that that this unit may represent the first fossil magma chamber of this type recognized in the geologic record.

INTRODUCTION

Rhyolite and dacite emplaced during supereruptions demonstrate that large volumes (>450 km^3) of eruptible silicic magma can exist in the upper crust. However, the time scales over which the magma reservoirs that source these eruptions are built are controversial. Thermal models suggest that magma emplacement rates need to be >0.003–0.01 km^3/yr in order to accumulate enough eruptible magma to supply a supereruption (Annen, 2009; Gelman et al., 2013). However, these rates are higher than the time-averaged rates for nearly all well-studied granitoid plutonic complexes (i.e., <0.001 km^3/yr; Glazner et al., 2004). This disparity contradicts evidence that supereruptions are sourced from crystal-rich magma chambers that should be preserved in the geologic record as granitoid plutons (e.g., Bachmann et al., 2007), leading to two end-member hypotheses for magma chamber construction: (1) that long-lived magma reservoirs spend the majority of their lifetimes at low melt fraction and can differentiate to form pools of eruptible magma or be rejuvenated through new magma input (Bachmann and Bergantz, 2003, 2004), or (2) that some silicic magma chambers are assembled rapidly and exist ephemerally within the upper crust (e.g., Glazner et al., 2004).

Geochronologic studies paired with robust volume estimates for magmatic intrusions provide the most direct means of assessing magma emplacement rates and quantifying crystallization duration, but the number of such studies is limited (e.g., Matzel et al., 2006; Tappa et al., 2011; Davis et al., 2012; Leuthold et al., 2012; Frazer et al., 2014; Barboni et al., 2015). Here we present new mapping and high-precision U-Pb zircon geochronology from the Golden Horn batholith (GHB) in the North Cascades, Washington State (USA). These data show that part of the batholith was assembled rapidly and may represent a fossil large-volume (>424 km^3) silicic magma chamber.

GOLDEN HORN BATHOLITH

The 307 km^2 Eocene GHB intrudes Mesozoic sedimentary, volcanic, and plutonic rocks near the southern end of the Coast Plutonic Complex (Fig. 1A). It is dominantly peralkaline and calc-alkaline granite and granodiorite with minor diorite. The presence of a narrow metamorphic aureole, abundant miarolitic cavities, and intrusive breccias point to emplacement within the upper crust. We estimate a depth of ~7–8 km based on compositions of GHB granite that plot near the 0.2 GPa water-saturated eutectic in the quartz-albite-orthoclase (Qz-Ab-Or) system (Fig. DR1 in the GSA Data Repository[1]) and a pressure of 0.25 ± 0.06 GPa calculated using Al-in-hornblende barometry (for methods and results, see the Data Repository).

Our geologic mapping and that of Stull (1969) split the GHB into (1) peralkaline granite; (2) hypersolvus granite; (3) rapakivi granite; (4) heterogeneous granite; (5) granodiorite; and (6) diorite (Figs. 1B and 1C; for petrographic descriptions, see the Data Repository); topographic relief of >2 km gives excellent three-dimensional control on unit geometry and shows that they form sheet-like bodies (Figs. 1B and 1C). Volumes were estimated by assuming that each sheet had a constant thickness and was tabular across its areal extent, including eroded portions where we can confidently project units across glacial valleys. (For the thicknesses and areas used for these estimates, see the Data Repository) The peralkaline and hypersolvus granites are exposed in a downdropped fault block in the southeastern part of the GHB (Fig. 1B), and we calculate volumes of 29 km^3 and 54 km^3, respectively, for these units. These volumes are likely minimums because they do not include any parts of these sheets that may have extended to the northwest, but are now eroded. A larger size for the hypersolvus granite is suggested by a <50-m-wide (not shown in Fig. 1B) zone of this unit exposed along the western side of the batholith. We assume that the rapakivi granite and heterogeneous granite extend under the entire areal extent of the granitoid portions of the GHB, resulting in volumes of >424 km^3 and 197 km^3, respectively. The volume of the rapakivi granite is a minimum estimate because the top and bottom of the sheet are not exposed within the same fault block (Fig. 1B). Volumes for the diorite and granodiorite were not estimated due to their limited exposure.

U-Pb ZIRCON GEOCHRONOLOGY

Our minimum volume estimates for the GHB provide an excellent opportunity to estimate magma emplacement rates, and we dated 15 samples using U-Pb zircon chemical abrasion–isotope dilution–thermal ionization mass spectrometry geochronology (Mattinson, 2005) with this goal in mind. (For the methods used for these analyses, see the Data Repository; measured isotopic data are in Table DR4, select zircon cathodoluminesence [CL] images are in Fig. DR3, and concordia plots are in Fig. DR6.) We use $^{206}Pb/^{238}U$ dates for all of our interpretations because this chronometer provides the most precise and accurate date for

[1]GSA Data Repository item 2016104, unit descriptions, methods and results for Al-in-hornblende barometry, zircon CL images and petrography, U-Pb geochronology methods, and Monte Carlo methods, is available online at www.geosociety.org/pubs/ft2016.htm, or on request from editing@geosociety.org or Documents Secretary, GSA, P.O. Box 9140, Boulder, CO 80301, USA.

GEOLOGY Data Repository item 2016104 | doi:10.1130/G37631.1

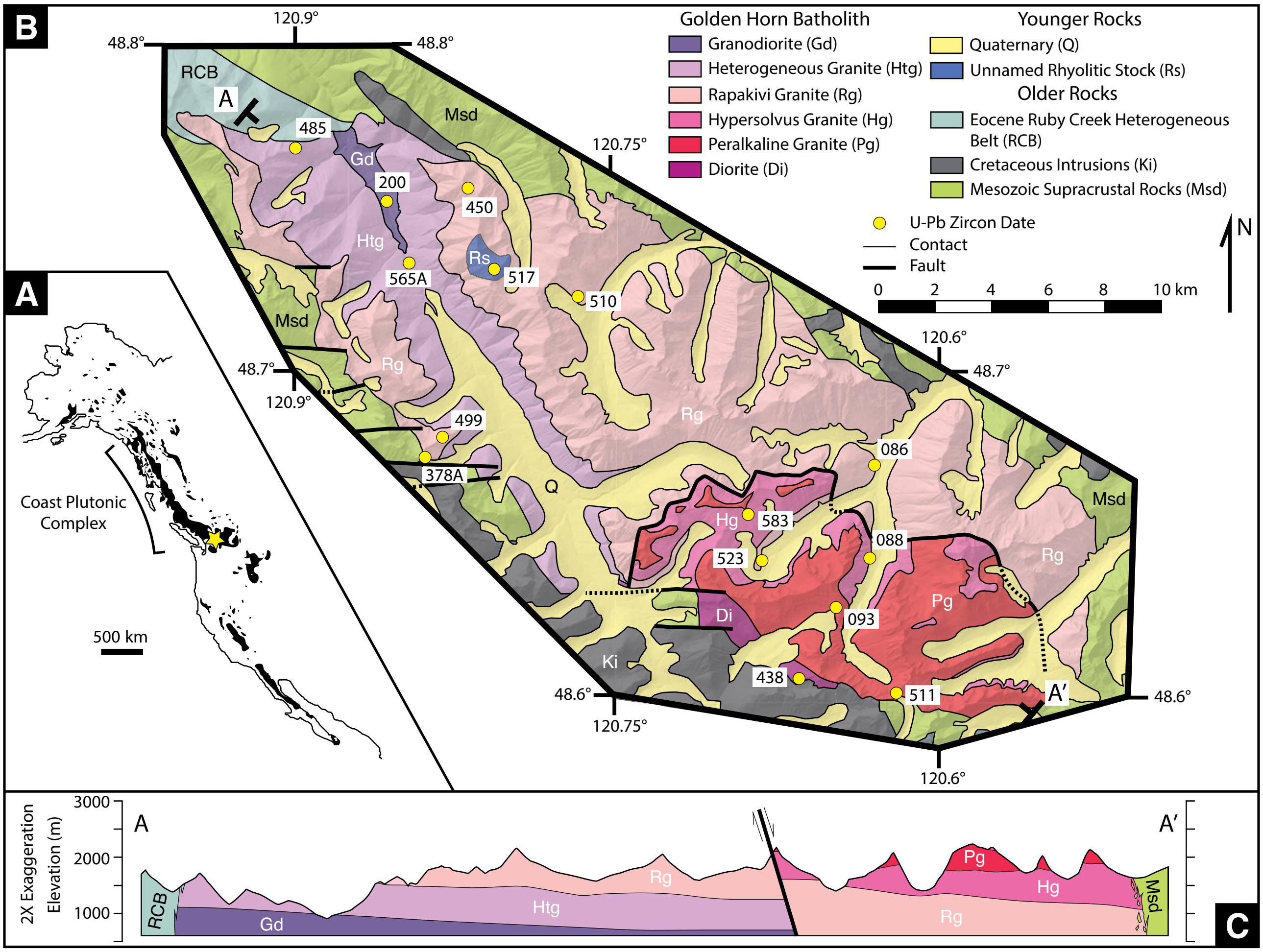

Figure 1. A: Map modified from Miller et al. (2000) showing the location of the Golden Horn batholith (GHB, yellow star) in relation to other Mesozoic and Paleogene plutonic rocks in the North American Cordillera (shown in black). B: Geologic map of the GHB. Internal contacts are based on our mapping and that of Stull (1969). External contacts are from Haugerud and Tabor (2009). The locations of samples dated by U-Pb zircon geochronology are shown with yellow circles. Sample names are abbreviated such that XXX should be read as NC-MPE-XXX. C: Cross section of the GHB along A-A′ showing the sheet-like nature of the mapped units

rocks of this age. Reported dates are corrected for initial disequilibrium in the ^{238}U-^{206}Pb decay chain using the measured $[Th/U]_{zircon}$ and the mean ratio of zircon/melt partition coefficients for Th and U ($f_{ThU} = 0.138$) from high-SiO_2 rhyolites erupted from the Yellowstone caldera (Stelten et al., 2015). The 2σ variability in the mean square weighted deviation (MSWD; Wendt and Carl, 1991) of weighted means is used to determine whether analytical uncertainty can account for the observed intrasample dispersion in zircon dates or whether it represents resolvable age differences in zircon crystallization. With the exception of a single antecrystic grain found in sample NC-MPE-485 (Fig. 2A), which is excluded from our calculations, none of the samples have resolvable age dispersion (Table 1). Therefore, we conclude that the duration of zircon crystallization within each hand sample is equal to or less than our analytical uncertainty (18–34 k.y.). Because all of the analyses used the same isotopic tracer and decay constants, all discussion of the data uses analytical uncertainty only.

The petrologic significance of zircon dates is dependent on when the melt became saturated with this mineral during its crystallization history. Early saturation can result in inherited zircons entrained from the magma's source region or antecrystic zircons that record crystallization at depth prior to transport and emplacement, leading to overestimates of the magma residence time in the upper crust (Miller et al., 2007; Barboni et al., 2015). Alternatively, late zircon saturation may lead to limited age dispersion that underestimates residence time. CL images of zircons from the GHB do not show inherited cores (Fig. DR3), and only one of the dated zircons is demonstrably antecrystic (Fig. 2A), suggesting that the majority of GHB magmas intruded at temperatures above zircon saturation (Miller et al., 2003). Furthermore, petrographic observations (Fig. DR4) demonstrate that zircon predated or cocrystallized with the major rock-forming minerals in each sample, and we consider the duration of zircon crystallization to approximate the duration of magma crystallization at the emplacement level.

The difference between the oldest and youngest dates within the GHB demonstrates that it was built over at least 739 ± 34 k.y. (Fig. 2A), starting with intrusion of the diorite and followed by downward accretion of the peralkaline granite, hypersolvus granite, rapakivi granite, and granodiorite sills. Subsequently, the heterogeneous granite intruded along the contact between the rapakivi granite and granodiorite, and a subvolcanic stock of uncertain relationship to the batholith intruded the rapakivi granite (Fig. 1B). Estimates for the duration of magmatism within individual units are reported in Figure 2A and represent the difference between the weighted mean dates of the oldest and youngest samples.

MAGMA CHAMBER CONSTRUCTION AND CRYSTALLIZATION

Magma emplacement rates were calculated assuming a constant rate of emplacement over our calculated durations. The duration magnitudes are

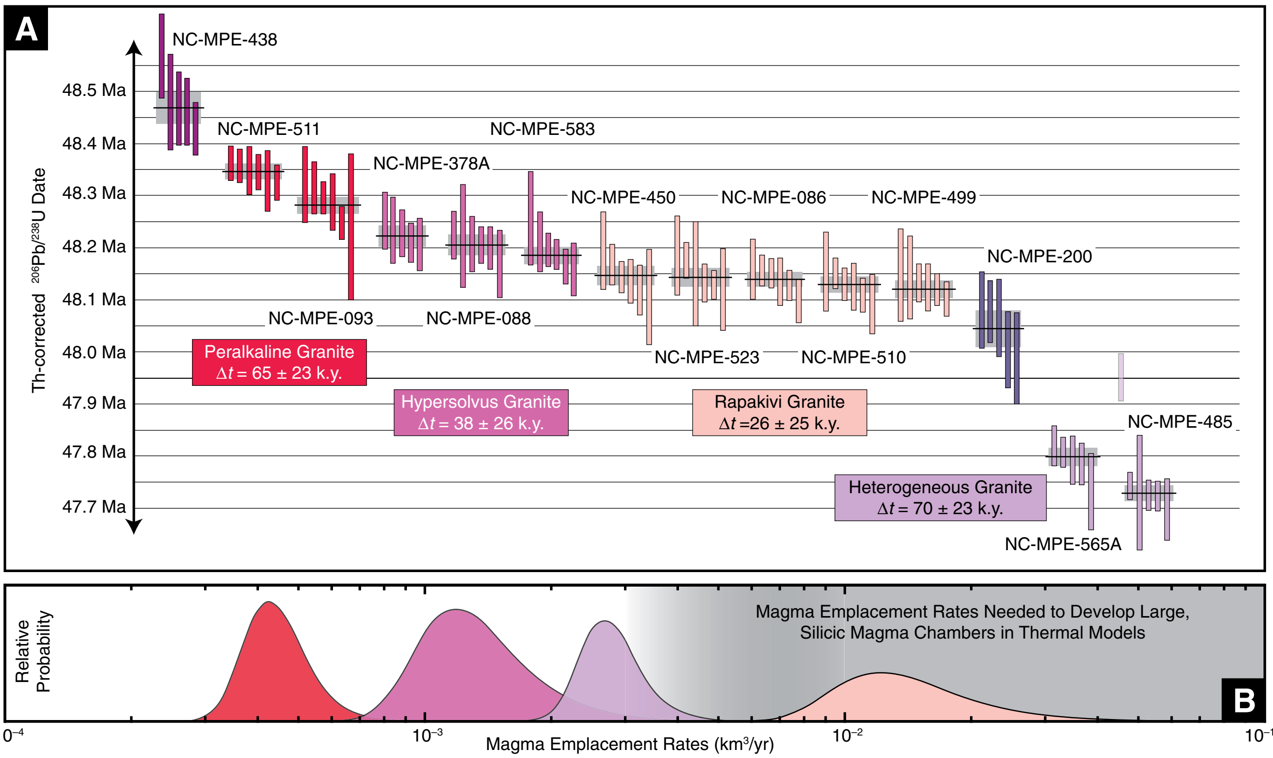

Figure 2. A: Rank order plot of Th-corrected ^{206}Pb/^{238}U zircon dates (bars represent 2σ analytical uncertainty) from the Golden Horn batholith (GHB). Colors correspond to map units and are the same as Figure 1B. Heavy black lines denote the weighted mean date for each sample reported with 2σ analytical uncertainty (gray boxes). For map units with more than one dated sample, we present the duration (Δ*t*) of magmatism calculated using the difference between weighted means of the oldest and youngest samples. B: Relative probability plots for magma emplacement rates within the GHB (colors as in Fig. 1B) calculated using Monte Carlo simulations (for methods, see the Data Repository [see footnote 1]). The heights of the curves are, respectively, scaled 1×, 5×, 5×, and 30× for the peralkaline, hypersolvus, heterogeneous, and rapakivi granites, to aid in comparison. The emplacement rates (>0.003–0.01 km^3/yr) needed to produce large volumes of eruptible silicic magma in thermal models (Annen, 2009; Gelman et al., 2013) are shaded gray.

similar to our analytical uncertainty and lead to asymmetric probability distributions for rates calculated using Monte Carlo simulations (Fig. 2B; for methods, see the Data Repository). Given this asymmetry, we report the mode of these distributions as the best estimate for the magma emplacement rate in each unit. The peralkaline (~0.0004 km^3/yr), hypersolvus (~0.0012 km^3/yr), and heterogeneous granite (~0.0027 km^3/yr) span the range of rates

TABLE 1. U-Pb ZIRCON GEOCHRONOLOGY RESULTS

Sample*	Weighted mean ^{206}Pb/^{238}U date† (Ma)
NC-MPE-438	48.468 ± 0.030/0.037/0.064 (n = 5, MSWD = 1.84)
NC-MPE-511	48.346 ± 0.015/0.026/0.058 (n = 6, MSWD = 0.69)
NC-MPE-093	48.281 ± 0.018/0.028/0.059 (n = 6, MSWD = 1.91)
NC-MPE-378A	48.223 ± 0.021/0.030/0.060 (n = 5, MSWD = 0.54)
NC-MPE-088	48.205 ± 0.020/0.030/0.060 (n = 6, MSWD = 0.42)
NC-MPE-583	48.185 ± 0.016/0.027/0.058 (n = 6, MSWD = 1.27)
NC-MPE-450	48.146 ± 0.018/0.028/0.059 (n = 6, MSWD = 1.08)
NC-MPE-523	48.144 ± 0.017/0.027/0.058 (n = 6, MSWD = 1.33)
NC-MPE-086	48.139 ± 0.014/0.025/0.057 (n = 6, MSWD = 1.44)
NC-MPE-510	48.129 ± 0.016/0.026/0.058 (n = 6, MSWD = 1.26)
NC-MPE-499	48.120 ± 0.017/0.027/0.058 (n = 6, MSWD = 0.50)
NC-MPE-200	48.045 ± 0.034/0.041/0.066 (n = 5, MSWD = 1.33)
NC-MPE-565A	47.799 ± 0.018/0.028/0.058 (n = 5, MSWD = 1.38)
NC-MPE-485	47.729 ± 0.015/0.026/0.057 (n = 5, MSWD = 0.64)
NC-MPE-517	<47.988 ± 0.052/0.056/0.076 (n = 1, maximum age)

*GPS locations for samples are presented in Table DR4 (see footnote 1).
†Corrected for initial Th/U disequilibrium using f_{ThU} = 0.138 (Stelten et al., 2015). Uncertainties are reported in the format ±X/Y/Z, where X is the analytical uncertainty, Y includes uncertainty in the EARTHTIME ^{205}Pb-^{235}U-^{238}U isotopic tracer (Condon et al., 2015; McLean et al., 2015), and Z includes uncertainty in the ^{238}U decay constant. MSWD—mean square of weighted deviates.

in other well-studied plutonic complexes (Fig. DR7), and distinct sample dates (Fig. 2A) and sharp internal contacts support the interpretation that these bodies never formed single, large-volume magma chambers. The rapakivi granite, however, has a calculated magma emplacement rate of 0.0125 km^3/yr, exceeding the rates required for the construction of large-volume silicic magma chambers in thermal models (Fig. 2B). While it is possible that our dates for this unit do not span its complete emplacement duration, overlapping zircon dates (Fig. 2A) from five widely spaced samples (Fig. 1B) indicate that melt was simultaneously present throughout most of the sheet. Because we infer that zircon crystallization occurred over a similar interval to that of magma crystallization, we suggest that this unit represents a large fossil silicic magma chamber. The 26 ± 25 k.y. duration of magma emplacement and crystallization implies that this body was an ephemeral feature and crystallized much faster than the crystallization time scales (>100 k.y.) predicted for silicic magma reservoirs the size of the rapakivi granite at ~5–10 km (Gelman et al., 2013). The reasons for such rapid crystallization are unknown, but may include the relatively short duration of high magma emplacement rates and the evolved nature of the melt (whole-rock SiO_2 ranges from 73 to 76 wt%; Stull, 1969).

Extremely high magma emplacement rates likely trigger eruptions by generating overpressure within magma chambers (e.g., Degruyter et al., 2016), and this may explain the scarcity of rapidly assembled silicic magma chambers in the plutonic record (e.g., Glazner et al., 2004; Tappa et al., 2011). It is currently unclear whether any part of the GHB is related to an eruption. In the Chumstick strike-slip basin, ~100 km to the south of the GHB, 9 tuffs closely match the batholith in age (Eddy et al., 2016), but the geochemical data needed to assess whether they are cogenetic do not exist. Nevertheless, the discovery of extremely high magma emplacement rates in the rapakivi granite of the GHB demonstrates that plutons representing rapidly assembled large-volume silicic magma chambers can be preserved in the geologic record, and we anticipate that more such fossil chambers will be discovered in the future.

CONCLUSIONS

New geologic mapping and high-precision U-Pb zircon geochronology from the Eocene GHB provide estimates of magma emplacement rates for four of six map units. The largest unit, a >424 km^3 body of rapakivi granite, was built over 26 ± 25 k.y., implying a magma emplacement rate of ~0.0125 km^3/yr. This is the highest rate documented in a granitoid pluton and exceeds the thermally modeled requirements for the development of large silicic magma chambers. We suggest that this unit represents the first fossil large-volume silicic magma chamber identified in the geologic record. The continued study and documentation of such chambers will provide unique opportunities to better understand the processes that occur within these chambers and their relationship to large eruptions.

ACKNOWLEDGMENTS

We thank B. Klein, M. Ibanez-Mejia, N. McLean, O. Jagoutz, and C. Scudder for discussions about data interpretation; A. Gregovich, D. Vassey, F. Paine, M. Carpenter, and T. LaCasse for field assistance; and E. Barry and J. Pu for laboratory assistance. This work was supported by National Science Foundation grants EAR-1118883 to Bowring, EAR-1119358 to Miller, and EAR-1119252 to Tepper. This paper benefited from insightful reviews by A. Glazner, O. Bachmann, and an anonymous reviewer, and the editorial handling of J. Spotila.

REFERENCES CITED

Annen, C., 2009, From plutons to magma chambers: Thermal constraints on the accumulation of eruptible silicic magma in the upper crust: Earth and Planetary Science Letters, v. 284, p. 409–416, doi:10.1016/j.epsl.2009.05.006.

Bachmann, O., and Bergantz, G.W., 2003, Rejuvenation of the Fish Canyon magma body: A window into the evolution of large-volume silicic magma systems: Geology, v. 31, p. 789–792, doi:10.1130/G19764.1.

Bachmann, O., and Bergantz, G.W., 2004, On the origin of crystal-poor rhyolites: Extracted from batholithic crystal mushes: Journal of Petrology, v. 45, p. 1565–1582, doi:10.1093/petrology/egh019.

Bachmann, O., Miller, C.F., and de Silva, S.L., 2007, The volcanic-plutonic connection as a stage for understanding crustal magmatism: Journal of Volcanology and Geothermal Research, v. 167, p. 1–23, doi:10.1016/j.jvolgeores.2007.08.002.

Barboni, M., Annen, C., and Schoene, B., 2015, Evaluating the construction and evolution of upper crustal magma reservoirs with coupled U/Pb zircon geochronology and thermal modeling: A case study from the Mt. Capanne pluton (Elba, Italy): Earth and Planetary Science Letters, v. 432, p. 436–448, doi:10.1016/j.epsl.2015.09.043.

Condon, D.J., Schoene, B., McLean, N.M., Bowring, S.A., and Parrish, R.R., 2015, Metrology and traceability of U-Pb isotopic dilution geochronology (EARTHTIME tracer calibration part I): Geochimica et Cosmochimica Acta, v. 164, p. 464–480, doi:10.1016/j.gca.2015.05.026.

Davis, J.W., Coleman, D.S., Gracely, J.T., Gaschnig, R., and Stearns, M., 2012, Magma accumulation rates and thermal histories of plutons of the Sierra Nevada batholith, CA: Contributions to Mineralogy and Petrology, v. 163, p. 449–465, doi:10.1007/s00410-011-0683-7.

Degruyter, W., Huber, C., Bachmann, O., Cooper, K.M., and Kent, A.J.R., 2016, Magma reservoir response to transient recharge events: The case of Santorini volcano (Greece): Geology, v. 44, p. 23–26, doi:10.1130/G37333.1.

Eddy, M.P., Bowring, S.A., Umhoefer, P.J., Miller, R.B., McLean, N.M., and Donaghy, E.E., 2016, High-resolution temporal and stratigraphic record of Siletzia's accretion and triple junction migration from nonmarine sedimentary basins in central and western Washington: Geological Society of America Bulletin, doi:10.1130/B31335.1.

Frazer, R.E., Coleman, D.S., and Mills, R.D., 2014, Zircon U-Pb geochronology of the Mount Givens Granodiorite: Implications for the genesis of large volumes of eruptible magma: Journal of Geophysical Research, v. 119, p. 2907–2924, doi:10.1002/2013JB010716.

Gelman, S.E., Gutierrez, F.J., and Bachmann, O., 2013, On the longevity of large upper crustal silicic magma reservoirs: Geology, v. 41, p. 759–762, doi:10.1130/G34241.1.

Glazner, A.F., Bartley, J.M., Coleman, D.S., Gray, W., and Taylor, R.Z., 2004, Are plutons assembled over millions of years by amalgamation from small magma chambers: GSA Today, v. 14, p. 4–11, doi:10.1130/1052-5173(2004)014<0004:APAOMO>2.0.CO;2.

Haugerud, R.A., and Tabor, R.W., 2009, Geologic map of the North Cascade range, Washington: U.S. Geological Survey Scientific Investigations Map 2940, scale 1:200,000, 52 p.

Leuthold, J., Muntener, O., Baumgartner, L.P., Putlitz, B., Ovtcharova, M., and Schaltegger, U., 2012, Time resolved construction of a bimodal laccolith (Torres del Paine, Patagonia): Earth and Planetary Science Letters, v. 325–326, p. 85–92, doi:10.1016/j.epsl.2012.01.032.

Mattinson, J.M., 2005, Zircon U-Pb chemical abrasion ("CA-TIMS") method: Combined annealing and multi-step partial dissolution analysis for improved precision and accuracy of zircon ages: Chemical Geology, v. 220, p. 47–66, doi:10.1016/j.chemgeo.2005.03.011.

Matzel, J.E.P., Bowring, S.A., and Miller, R.B., 2006, Time scales of pluton construction at differing crustal levels: Examples from the Mount Stuart and Tenpeak intrusions, North Cascades, Washington: Geological Society of America Bulletin, v. 118, p. 1412–1430, doi:10.1130/B25923.1.

McLean, N.M., Condon, D.J., Condon, B., and Bowring, S.A., 2015, Evaluating uncertainties in the calibration of isotopic reference materials and multi-element isotopic tracers (EARTHTIME tracer calibration II): Geochimica et Cosmochimica Acta, v. 164, p. 481–501, doi:10.1016/j.gca.2015.02.040.

Miller, C.F., McDowell, S.M., and Mapes, R.W., 2003, Hot and cold granites? Implications of zircon saturation temperatures and preservation of inheritance: Geology, v. 31, p. 529–532, doi:10.1130/0091-7613(2003)031<0529:HACGIO>2.0.CO;2.

Miller, J.S., Matzel, J.E.P., Miller, C.F., Burgess, S.D., and Miller, R.B., 2007, Zircon growth and recycling during the assembly of large, composite arc plutons: Journal of Volcanology and Geothermal Research, v. 167, p. 282–299, doi:10.1016/j.jvolgeores.2007.04.019.

Miller, R.B., Paterson, S.R., DeBari, S.M., and Whitney, D.L., 2000, North Cascades Cretaceous crustal section: Changing kinematics, rheology, metamorphism, pluton emplacement and petrogenesis from 0 to 40 km depth, *in* Woodsworth, G.J., et al., eds., Guidebook for geological field trips in southwestern British Columbia and northern Washington: Vancouver, Geological Association of Canada, p. 229–278.

Stelten, M.E., Cooper, K.M., Vazquez, J.A., Calvert, A.T., and Glessner, J.J.G., 2015, Mechanisms and timescales of generating eruptible rhyolitic magmas at Yellowstone caldera from zircon and sanidine geochronology and geochemistry: Journal of Petrology, v. 56, p. 1607–1642, doi:10.1093/petrology/egv047.

Stull, R.J., 1969, The geochemistry of the southeastern portion of the Golden Horn batholith, Northern Cascades, Washington [Ph.D. thesis]: Seattle, University of Washington, 127 p.

Tappa, M.J., Coleman, D.S., Mills, R.D., and Samperton, K.M., 2011, The plutonic record of a silicic ignimbrite from the Latir volcanic field, New Mexico: Geochemistry, Geophysics, Geosystems, v. 12, Q10011, doi:10.1029/2011GC003700.

Wendt, I., and Carl, C., 1991, The statistical distribution of the mean square weighted deviation: Chemical Geology, v. 86, p. 275–285, doi:10.1016/0168-9622(91)90010-T.

Manuscript received 23 December 2015
Revised manuscript received 28 February 2016
Manuscript accepted 29 February 2016

Printed in USA